Large-Scale Testing and Analysis of Concrete Encased Steel Coupling Beams under High Ductility Demands

C.J. Motter & J.W. Wallace
University of California, Los Angeles

R. Klemencic, J.D. Hooper & D.C. Fields
Magnusson Klemencic Associates, Seattle

SUMMARY:
Concrete encased steel coupling beams are an alternative to reinforced concrete coupling beams. Because prior testing has been conducted on relatively small steel sections, testing of large-scale specimens was conducted to validate analytical models used to determine the required embedment length. The test set-up included reversed-cyclic shear loading applied to the tip of a cantilevered coupling beam containing a structural steel section embedded into a reinforced concrete shear wall, which was simultaneously subjected to reversed-cyclic lateral loading to create alternating tension and compression fields across the embedment zone. To assess the degree of potential conservatism in the previously published embedment equations, tests were conducted on two composite coupling beams with varying embedment length, one beam with embedment length expected to result in good performance and a second beam with an embedment length of 75% of the first beam. Both test beams maintained shear coupling loads above 75% of the peak value up to a 6% rotation, although the beam with longer embedment displayed less strength degradation and less pinching.

Keywords: Coupling Beam, Link Beam, Composite Beam, Embedded Steel Section, Coupled Wall

1. INTRODUCTION

Reinforced concrete shear walls provide an efficient lateral system for resisting seismic and wind loads. Coupling beams connect adjacent colinear shear walls to create larger shear wall assemblages which more efficiently resist lateral loads. The coupling action of these beams reduces the overturning demand within individual wall piers, and imparts vertical forces to the walls via beam shear, thereby creating axial tension-compression couples between coupled wall piers. During significant seismic events, coupling beams are often the first elements to yield. For this reason, coupling beams act as fuses which dissipate earthquake energy through large inelastic rotations, and help control the magnitude and pattern of forces felt by the coupled walls.

ACI 318-11 code provisions require the use of diagonal reinforcement in reinforced concrete coupling beams when shear demand is high and length-to-depth ratio is low. Testing shows that beams constructed with this reinforcement maintain reliable strength during larger rotations (Naish et al, 2009). Such beams are frequently used in mid- and high-rise buildings in high seismic zones. Coupling beams are typically located between vertically stacked door or corridor openings, putting limitations on beam depth. The congestion associated with embedding diagonal reinforcement into boundary zones of reinforced concrete shear walls creates constructability challenges, thereby increasing construction time and cost.

The use of concrete encased steel coupling beams provides a viable design alternative and potentially decreases congestion in the wall boundary zone. Embedded steel sections transfer coupling forces to

shear walls through a bearing mechanism, which avoids the need for welded and bolted connections while benefiting from the ductility of properly selected structural steel sections. Steel wide-flange sections encased in concrete are provided further stability against buckling, which results in increased beam ductility.

2. BACKGROUND

For reinforced concrete coupling beams with embedded steel sections, the strength of the beam-to-wall connection is dependent on the embedment length of the steel section. Adequate embedment length may be defined as the length necessary to create reliable transfer of forces from the beam to the wall without excessively damaging the wall. Although no specific design guidelines are provided by codes, Mattock and Gaafar (1980) and Marcakis and Mitchell (1982) developed load transfer models to determine the required embedment length. Although these embedment models govern the transfer of forces from unencased cantilevered steel sections to reinforced concrete columns, the mechanism is parallel to the transfer of forces from steel coupling beams to reinforced concrete shear walls.

The Marcakis and Mitchell (1980) and Mattock and Gaafar (1982) embedment models both assume a linear strain distribution in the embedment region, with a strain of ε_c = 0.003 at the outer face of the connection, as shown in Figure 1. A uniform magnitude stress block is used to approximate the bearing stress distribution at the front of the embedment region, while a parabolic stress-strain relationship (Hognestad, 1955) is used to determine the bearing stress distribution along the deeper portion. Based on the applied beam shear, equilibrium is achieved through iteration by varying the strain gradient. In lieu of iteration, simplifying assumptions were used to develop design equations. Because both embedment models are based on the same assumptions (leading to identical stress diagrams), the Marcakis and Mitchell (1980) and Mattock and Gaafar (1982) design equations yield nearly identical results.

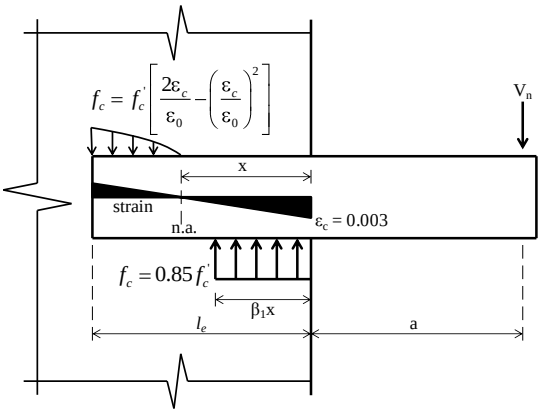

Figure 1. Embedment Model

Harries et al (2000) recommend that both the Marcakis and Mitchell (1980) and the Mattock and Gaafar (1982) embedment equations be modified to include the effects of concrete spalling at the face of the embedment. The Marcakis and Mitchell (1980) embedment equation modified to including spalling is as follows:

$$V_n = \frac{0.85 f_c' b(l_e - c)}{1 + 3.6\left(\frac{e}{(l_e - c)}\right)} \tag{2.1}$$

where $e=(a + c)+(l_e - c)/2$. V_n is the ultimate beam load, a is the cantilever length, l_e is the embedment length, c is the distance of spalling, b is the effective width, and f'_c is the maximum compressive stress of concrete. During testing, Marcakis and Mitchell (1980) observed spalling of cover concrete to the outside of the column confining ties in the connection region, indicating load spreading to this effective width. The effective width, b, is thus taken as the width of the confined region, measured to the outside of wall boundary hoops and ties, not to exceed 2.5 times the width of the embedded member. The distance of spalling at the face of the connection, c, is typically assumed to be equal to the depth of wall cover.

The Mattock and Gaafar (1982) embedment equation modified to including spalling is as follows:

$$V_n = 0.85 f_c' \left(\frac{t}{b} \right)^{0.66} \beta_1 b (l_e - c) \left(\frac{0.58 - 0.22\beta_1}{0.88 + (a+c)/(l_e - c)} \right) \tag{2.2}$$

where t is the wall thickness, b is the bearing width, equal to the flange width for wide-flange sections, and β_1 is the ACI stress block factor, defined as the ratio of the uniform stress block depth to the neutral axis depth.

Based on test results for shear-controlled composite coupling beams, Gong and Shahrooz (2001) recommend computing the embedment length necessary to develop the full expected capacity of the composite coupling beam, including the effects of encasement on shear strength. Significant embedment damage occurred for members in which encasement was neglected when determining the member capacity for computing embedment length.

3. TEST SET-UP AND SPECIMEN DESIGN

Prior tests conducted to assess the reliability of the embedment equations for composite coupling beams were commonly conducted at relatively small-scale. The reliability associated with extrapolating results of small-scale tests to prototypes has been questioned by the profession, particularly given the experience with fully-restrained welded-flange steel moment frame connections in the 1994 Northridge Earthquake. This research study strives to assess the reliability of embedment equations at the largest scale possible based on laboratory constraints (determined to be about one-half scale). Prior tests were often conducted for steel sections embedded into either uncracked (sometimes unstressed) walls or unstressed reaction blocks. Because local stress/strain fields could impact the required length of embedment, the test was designed to include a wall subjected to lateral loading and overturning moment such that the wall stresses at the embedment location represent realistic conditions.

The overall test set-up is shown in Figure 2. The test specimen consisted of a reinforced concrete shear wall with two one-half-length composite coupling beams (one on each side of the wall), which were tested individually (about a month apart). Each composite coupling beam contained a steel wide-flange section embedded into the shear wall. The only difference between the two coupling beams was the embedment length. An 890-kN (max.) actuator with +/- 152 mm stroke is used to apply vertical load to the one-half-length cantilever coupling beam. The point of load application represents the midpoint, which is also an inflection point, in a full-length coupling beam.

To generate wall overturning moment, two 1780-kN (max.) actuators with +/- 457 mm stroke are used to apply equal and opposite vertical loads. The wall lateral shear force (and additional moment) is applied by a 1335-kN (max.) actuator with +/- 305 mm stroke. To support the lateral reaction from the 1335-kN actuator, reaction blocks were stacked, grouted at the interfaces, and post-tensioned to the laboratory strong-floor with 31.75 mm diameter high-strength Dywidag rod. The “top beam” in Figure 2 refers to a

thickened portion at the top of the shear wall (poured continuously with the upper wall) constructed to facilitate anchorage to the steel loading beam (positioned across the top of the specimen). The top beam and footing were post-tensioned to the steel loading beam and the laboratory strong floor, respectively.

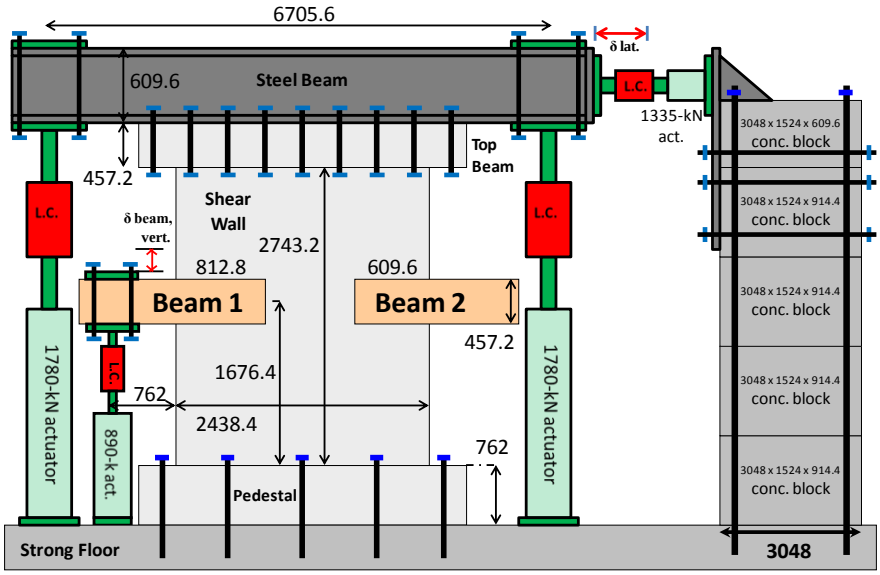

Figure 2. Schematic of the Overall Test Set-Up (all dimensions in mm)

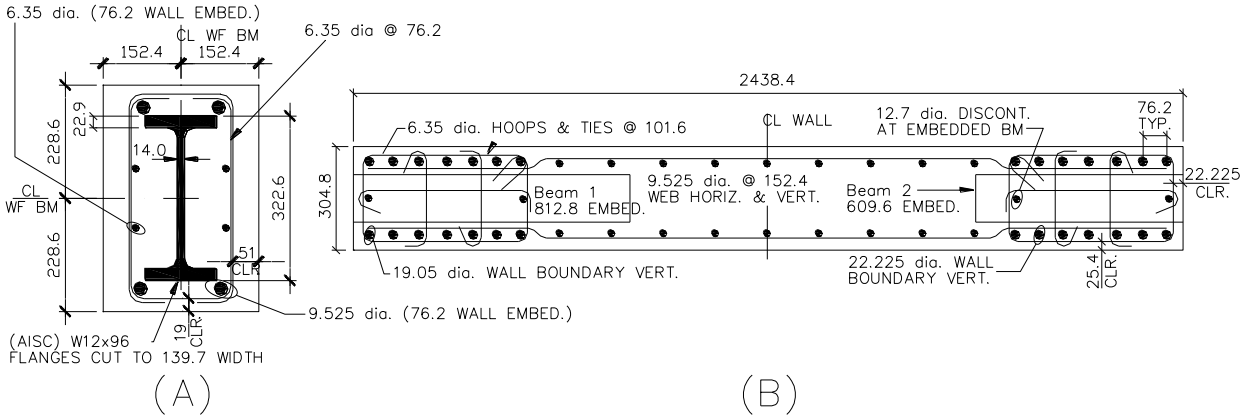

Figure 3. Beam (A) and Wall (B) Cross-Sections (all dimensions in mm)

Figure 3 shows cross-sections for the beams (same for both) and the shear wall. The embedded steel section was a (AISC) W12x96 (d = 322.6 mm, t_w = 14.0 mm, b_f = 309.9 mm, and t_f = 22.9 mm) with flanges trimmed to a width of 139.7 mm, which is an approximation of a one-half-scale (AISC) W24x250 (d = 668.0 mm, t_w = 26.4 mm, b_f = 335.3 mm, and t_f = 48.0 mm). One-half-scale represents the maximum feasible scale due to laboratory constraints. This scale was used to guide the sizing and detailing of the shear wall and coupling beams. The use of a built-up section for the embedded member was also considered in order to achieve precise scaling. However, due to differences in fabrication and material properties for wide-flange sections and built-up sections, the use of a built-up test section to represent a wide-flange prototype section was deemed undesirable.

The dimensions of the embedded steel section suggested 304.8 mm by 457.2 mm reinforced concrete encasement, which is consistent with an assumed 609.6 mm by 914.4 mm prototype. This led to a 762.0 mm cantilever length (to the point of load application) for the one-half-length test beam, assuming a coupling beam aspect ratio of 3.33, which is typical for high-rise office buildings in the United States. Due to the high aspect ratio, the beams were flexure-controlled. Because the contribution of concrete shear strength was not essential to ensure flexure-critical behavior, coupling beam stirrups (6.35 mm dia. @ 76.2 mm spacing) were detailed as two U-bars rather than individual hoops for ease of constructability. Coupling beam longitudinal bars (9.525 mm dia.), used as placeholders for shear reinforcement, were not developed in the shear wall, thereby contributing no flexural strength to the coupling beam to better control the moment transferred to the embedment region.

Table 1 shows the maximum achievable shear load, V_n, for the cantilevered composite beam and the corresponding required embedment length computed using different design methods for a range of structural steel properties. Because the beams are flexure-controlled, the maximum achievable shear load was obtained by dividing the ultimate flexural capacity by the cantilever length (including wall spalling, i.e. wall cover). This approach assumes that the intended yield and failure mechanism is entirely within the beam rather than the wall, meaning that beam failure occurs at the face of the embedment rather than in the connection. Based on the maximum achievable shear load, the required embedment length was determined using both the Marcakis and Mitchell (1980) and Mattock and Gaafar (1982) embedment equations corrected to include the effects of wall spalling per the recommendation of Harries et al (2000).

The two design methods used to compute the ultimate flexural capacity for the composite coupling beam were taken from AISC and ACI. For the AISC approach, the ultimate flexural capacity was computed based on a fully plastic steel section (using F_u) and a uniform stress block for concrete in compression. Variation of the AISC approach using a fully yielded section (using F_y) rather than fully plastic was also used for computation of member capacity. For the ACI approach, the steel section was converted into an equivalent area of reinforcement and reinforced concrete beam analysis was performed using BIAX software to determine the ultimate capacity. The steel properties used in the analyses were obtained from the test results of Liu et al (2007), which are used in the 2010 AISC *Seismic Provisions for Structural Steel Buildings*. These test results provide a mean and standard deviation, as well as a maximum and minimum, for actual yield stress, F_y, and ultimate stress, F_u, of structural steel wide flange sections tested under cyclic loading. Both the AISC and ACI methods assume monotonic loading and the development of full composite action (i.e. no slip) between the concrete and steel. Since cyclic loading is applied and shear studs have not been provided, these analysis methods are expected to over-predict the actual member capacity, which is conservative for computing minimum embedment lengths.

Table 1. Member Capacity and Corresponding Embedment Length

			μ-2σ	μ-σ	μ	μ+σ	μ+2σ	min	max	des. w/o ϕ	des. w ϕ
BIAX	Vn	kN	807	839	871	903	934	811	959	810	900
	Embed. (M&M)	mm	686	704	719	734	752	688	762	688	734
	Embed. (M&G)	mm	673	704	706	721	737	676	749	676	721
AISC, Fy	Vu	kN	696	730	763	797	830	702	854	702	780
	Embed. (M&M)	mm	627	645	663	681	699	630	711	630	673
	Embed. (M&G)	mm	615	632	650	668	686	617	696	617	660
AISC, Fu	Vu	kN	908	942	977	1011	1045	892	1099	884	982
	Embed. (M&M)	mm	737	754	772	787	805	729	831	726	775
	Embed. (M&G)	mm	724	742	759	775	792	716	818	711	762

Based on the range of required embedment lengths shown in Table 1, a conservative embedment length of 812.8 mm was selected for the first coupling beam. An embedment length of 609.6 mm was selected for the second coupling beam, in order to assess the degree of conservatism inherent in the embedment

equations and better understand the limitations of the connection. From this point forward, the beams with 812.8 mm and 609.6 mm embedment lengths are referred to as Beam 1 and Beam 2, respectively.

Figure 3(b) shows the shear wall cross-section. ACI 318-11 Chapter 21 and Appendix A (strut-and-tie modeling) code provisions were used to guide the design of the shear wall. Within the embedment zone, bearing forces are assumed to transfer from wall concrete into wall vertical reinforcement. Because the bearing forces were computed to be larger for the section with shorter embedment length (Beam 2), local stresses in wall vertical boundary bars were expected to be larger than those associated with the longer embedment length (Beam 1). For this reason, 14#7 (22.225 mm dia.) wall verticals were used on the side with Beam 2, and 14#6 (19.05 mm dia.) wall verticals were used on the side with Beam 1. After completion of the coupling beam tests, the shear wall was tested to failure.

An intermediate level of wall boundary confinement is representative of a mid-to-upper-level story for a high-rise reinforced concrete building in a zone of moderate to high seismic risk. Transverse reinforcement at the wall boundary was provided to satisfy code provisions for an intermediate level of boundary confinement, namely ACI 318-11 Section 21.9.6.5, which requires a 203.2 mm maximum spacing. Assuming 12.7 mm hoops and ties at 203.2 mm spacing for the prototype suggested 6.35 mm hoops and ties at 101.6 mm spacing for the test specimen. ACI 318-11 Section 21.9.6.5 also requires that $h_x \leq$ 355.6 mm (per ACI 318-11 Section 21.6.4.2 as mandated within ACI 318-11 Section 21.9.6.5), which scaled to $h_x \leq$ 177.8 mm. h_x is defined as the maximum center-to-center spacing of cross-ties or hoop legs. Two cross-ties were used for the test specimen in the short direction as shown in Figure 3; therefore, h_x = 180.975 mm for the 22.225 mm (dia.) verticals (deemed close enough to 177.8 mm). A central cross-tie was also needed in the long direction. Discontinuous 12.7 mm (dia.) vertical bars were used as placeholders for this cross-tie, but were not embedded into the footing or the concrete top beam in order to avoid adding wall flexural strength. For horizontal and vertical web bars the code minimum reinforcement ratio is ρ=0.0025 per ACI 318-11 Section 21.9.2.1. At one-half-scale, 19.05 mm (dia.) @ 304.8 mm spacing (ρ=0.0031) scaled to 9.525 mm (dia.) @ 152.4 mm spacing (ρ=0.0031).

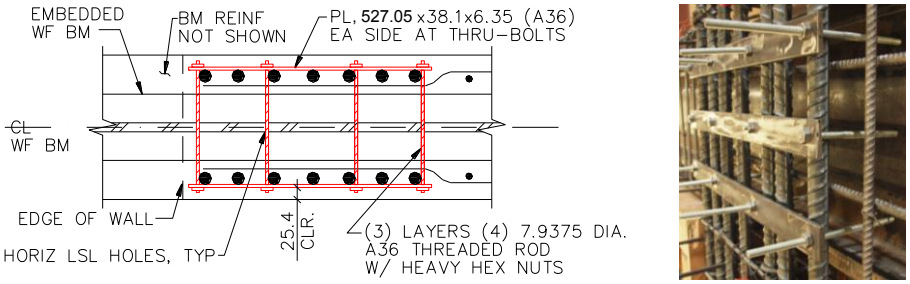

Figure 4. Wall Boundary Embedment Detailing (all dimensions in mm)

Figure 4 shows the wall boundary detailing at the connection zone. Due to the presence of the embedded steel section, standard hoops and cross-ties cannot be placed. In order to re-establish wall boundary confinement through the depth of the embedded beam, pre-drilled holes through the web of the steel section allowed the use of threaded through-rods and steel plates to achieve the desired level of confinement.

The specimen was constructed in three concrete pours, namely footing, lower wall (to the top of the coupling beam), and upper wall. Cylinder data for the lower wall pour was used to determine actual material properties for concrete in the coupling beams. For Beam 1, f'_c = 51.0 MPa and ε_0 = 0.0027. For Beam 2, f'_c = 51.0 MPa and ε_0 = 0.0029. The embedded steel sections were cut from the same (AISC) W12x96. Six test coupons were cut from this source member (three from the flanges and three from the web); however, test data for structural steel is unavailable at this time.

4. TESTING PROTOCOL

The testing protocol is shown in Figure 5. The coupling beam actuator controlled the test. The three wall actuators were slaved to this actuator based on the force ratios shown in Figure 5. For Beam 1 the wall forces were large enough to exceed the wall cracking moment at the embedment zone. For Beam 2 the wall forces were 2.5 times larger than for Beam 1 in order to approach wall yield at the embedment zone. Larger walls loads in combination with short embedment length were expected to create the most critical scenario for the coupling beam connection.

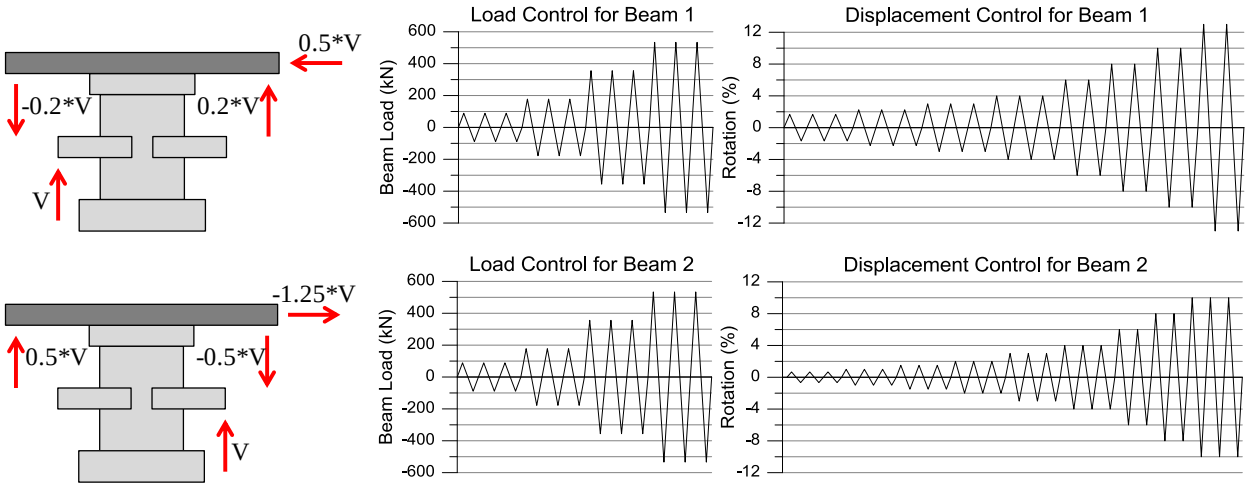

Figure 5. Testing Protocol

The calculated shear force at yield (based on BIAX analysis using average steel yield stress, F_y, and ultimate stress, F_u) for the composite coupling beam was computed to be 711.7 kN. Load-controlled cycles were performed at increments of $V_y/8$, $V_y/4$, $V_y/2$, and $3V_y/4$. Based on the observed stiffness at $3V_y/4$, the yield rotation was estimated and the test proceeded as displacement-controlled. For Beam 1 the yield rotation was estimated to be 1.67%, and subsequent cycles were carried out at rotations of 1.67%, 2.25%, 3.0%, 4.0%, 6.0%, 8.0%, 10.0%, and 13.0%. Despite very little strength degradation, the test was stopped at 13.0% rotation, which was deemed larger than any practical performance goal.

The difference in stiffness between the positive (upward) and negative (downward) loading direction was significant for Beam 2. Therefore, during load-controlled cycles, loading in the negative direction was carried out under displacement-control based on the actual displacement for the positive direction (which was load-controlled). Yield rotation in the positive direction was estimated to be 0.6%, and subsequent displacement-controlled cycles were carried out at rotations of 0.67%, 1.0%, 1.5%, 2.0%, 3.0%, 4.0%, 6.0%, 8.0%, and 10.0%.

5. TEST RESULTS

Although significant outward slip of the steel section was observed during the tests, in actual structures, outward slip of the steel section is restrained at some level by a floor slab as well as embedment into an adjacent shear wall, which creates axial load on the coupling beam. Because axial load is dependent on structural lay-out, geometry, etc., it was not simulated for this test due to the lack of a specific prototype.

Figure 6 shows load-displacement plots for Beam 1 and Beam 2. Beam 1 displays excellent ductility with minimal strength degradation up to 13% rotation, while Beam 2 displays less capacity, more pinching,

and greater strength degradation. This is consistent with observed embedment damage and is attributable to the difference in embedment length. The asymmetry in the load-displacement plot for Beam 2 is attributable to the stress field created at the embedment zone due to wall loading. During positive (upward) beam loading, the wall loads create a vertical compression field in the embedment region, while a tension field is induced in the wall during negative (downward) beam loading. This results in a beam connection which is softer and develops less capacity when in tension compared to compression.

Throughout testing of Beam 1, a correction to the measured displacement was made to account for beam displacement due to wall rotation. This was also done for the early phases of Beam 2 testing; however, the data were not reliable and the idea of correcting for this was abandoned. Test data for Beam 1 were adjusted to neglect the correction in order to provide a direct comparison with Beam 2 test data in Figure 6. For this reason, the load-rotation plot for Beam 1 in Figure 6 shows rotation levels that differ slightly from those used to control the test.

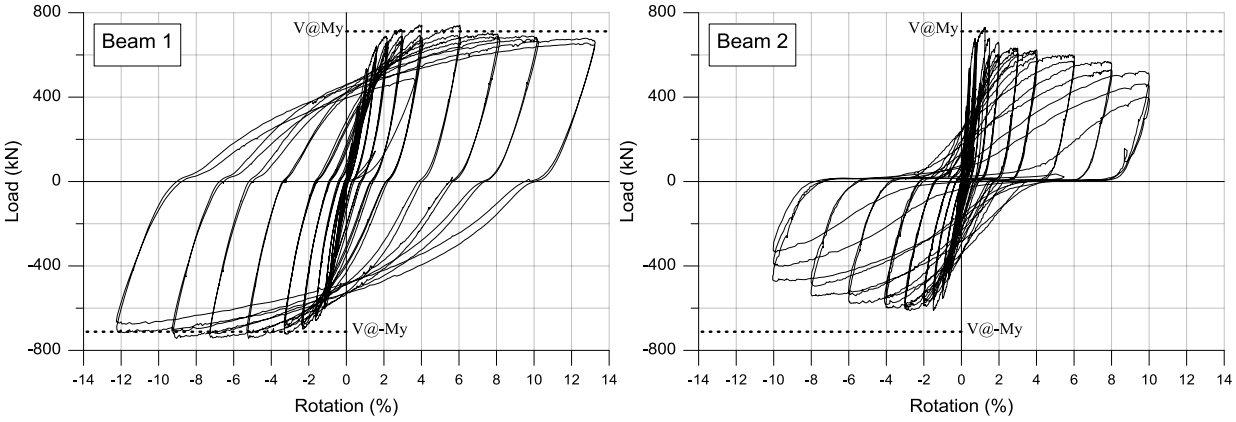

Figure 6. Beam Load v. Rotation

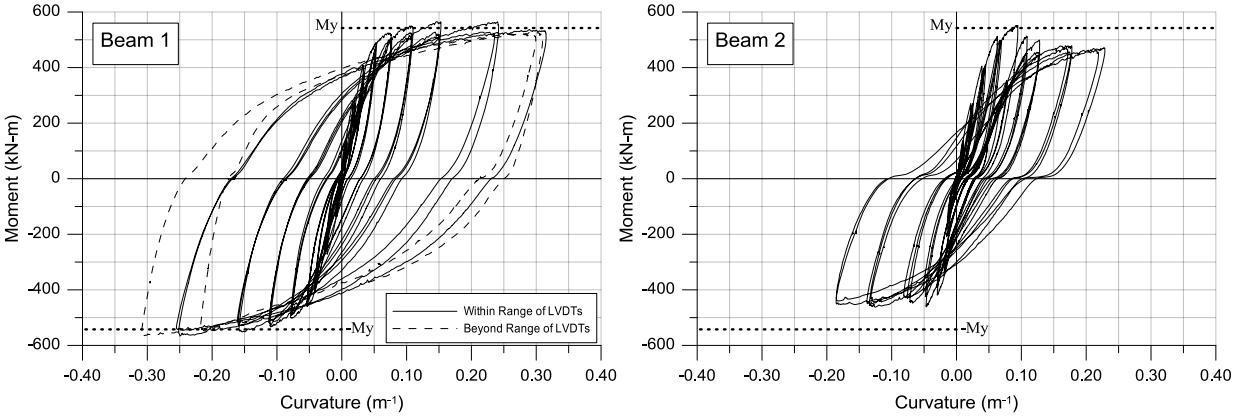

Figure 7. Beam Moment v. Curvature

Figure 7 compares moment-curvature plots at the beam-wall interface for Beam 1 and Beam 2. For Beam 1, the data are reliable up to 8% rotation, at which point the data become questionable (although stable) due to exceedance of the linear range of the LVDTs. For Beam 2, the data are reliable up to 4% rotation at which point the data become unstable due to the exceedance of the LVDT stroke. Referring to Figure 7, the plot for Beam 1 is relatively symmetric with minimal pinching. For Beam 2 the curvature is larger for positive loading than negative, which suggests more beam yielding and less connection deformation for the positive direction compared to the negative. Strain data for Beam 1 and Beam 2 indicate a lack of

plastic hinge propagation outward into the cantilever. The moment-curvature data in Figure 7 indicate the concentration of significant plastic rotation at the interface, which is consistent with observed damage patterns. The values related to yield moment, namely $V@M_y$ and M_y, shown in Figure 6 and Figure 7, respectively, were based on BIAX analysis using average steel properties.

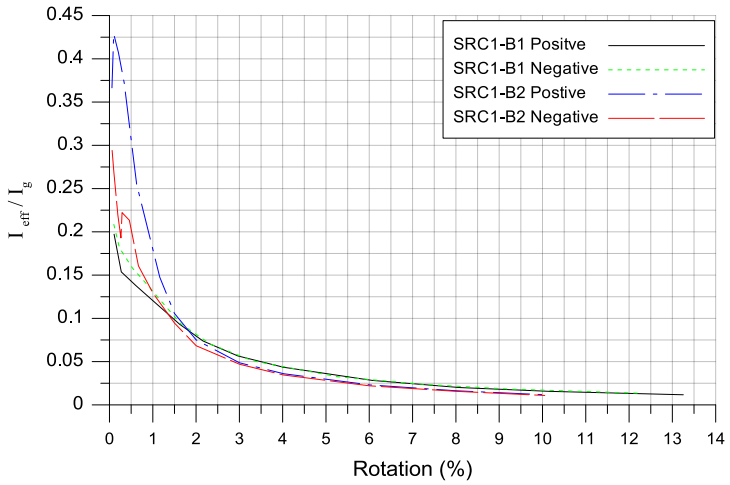

Figure 8. Beam Effective Stiffness

Figure 8 shows a plot of effective stiffness for Beam 1 and Beam 2 for both positive and negative loading. For comparative purposes, the absolute value of rotation is used, putting all data in the first quadrant. The effective secant stiffness values in this plot were computed at the peaks (positive and negative) of the load-displacement plot (figure 6) for the first loading cycle at each increment, using the equation for a point load on a fixed cantilever.

Referring to Figure 8, there is minimal difference in the effective secant stiffness beyond rotations of about 1.5%. For rotations less than 1.5%, the difference between positive and negative stiffness values for Beam 2 is attributable to the embedment stresses in the wall, which produce compression for positive loading and tension for negative loading. The effective stiffness appears largest for Beam 2 loaded in the positive direction. Even though the embedment length is shorter, the wall loads are larger, and the stiffness is larger due to the confining effect produced by larger wall compression in the embedment zone.

The larger negative stiffness for Beam 2 compared to Beam 1 is interesting. Although it could simply be due to the inherent variability associated with testing, it could also be due to wall rotation. The applied wall loads create rotation which generates beam displacements that oppose the measured displacements reflected in Figure 8. Therefore, the relative cantilever displacement includes the measured displacement plus any additional opposing displacement due to wall rotation. Because the plot in Figure 8 does not reflect the effect of wall rotation, the stiffness values are inflated. Since the wall loads for Beam 2 were 2.5 times larger than for Beam 1, the effect is more pronounced for Beam 2, which may explain the larger effective stiffness in the negative direction.

6. CONCLUSIONS

A testing program was undertaken to assess the performance of concrete encased steel coupling beams embedded into reinforced concrete shear walls at a realistic scale. Wall loading was simulated to create stress fields in the embedment zone that are consistent with actual structures. Two tests were conducted on embedded wide-flange sections of varying embedment length. The embedment models of Marcakis

and Mitchell (1980) and Mattock and Gaafar (1982) were used to compute the required embedment length needed to transfer bearing forces from the beam to the wall without damaging the connection. The embedment length for Beam 1 was intended to represent a conservative design based on available information. The embedment length for Beam 2 was set to 75% of the value for Beam 1 to assess the conservatism inherent in the aforementioned approach. Wall loads were 2.5 times larger for Beam 2 than Beam 1, nearly reaching yield at the embedment zone.

The test results indicate excellent performance for Beam 1, with applied beam rotation capacity exceeding 10% with almost no strength degradation. The tip load for Beam 2 dropped to approximately 75% of the peak load at 6% beam rotation, and more pinching was observed in the load-deformation response. Because larger wall compression at the embedment region is not expected to degrade the connection, direct comparison of Beam 1 and Beam 2 in the positive loading direction suggests that the difference in embedment length rather than wall loading is primarily responsible for the difference in performance. Additional tests are planned to further assess design requirements and to assess possible alternative composite beam configurations.

ACKNOWLEDGEMENT

The work presented in this paper was supported by funds from the Charles Pankow Foundation. This research was performed in a collaboratory renovated with funds provided by the National Science Foundation under Grant No. 0963183, which is an award funded under the American Recovery and Reinvestment Act of 2009 (ARRA). Any opinions, findings, and conclusions expressed in this material are those of the authors and do not necessarily reflect those of the National Science Foundation.

REFERENCES

ACI Committee 318. (2011). Building Code Requirements for Structural Concrete (ACI 318-11) and Commentary, American Concrete Institute, Farmington Hills, MI.

AISC. (2005). Steel Construction Manual, 13th edition. American Institute of Steel Construction, Inc., Chicago, IL.

AISC. (2010). Seismic Provisions for Structural Steel Buildings. ANSI/AISC 341-05, American Institute of Steel Construction, Chicago, IL.

Gong, B. and Shahrooz, B.M. (2001). Steel-Concrete Composite Coupling Beams – Behavior and Design. *Engineering Structures*. 23(11), 1480-1490.

Gong, B. and Shahrooz, B.M. (2001). Concrete-Steel Composite Coupling Beams. I: Component Testing. *Journal of Structural Engineering*. 127:6, 625-631.

Gong, B. and Shahrooz, B.M. (2001). Concrete-Steel Composite Coupling Beams. II: Subassembly Testing and Design Verification. *Journal of Structural Engineering*. 127:6, 632-638.

Harries, K.A., Gong, B. and Shahrooz, B.M. (2000). Behavior and Design of Reinforced Concrete, Steel, and Steel-Concrete Coupling Beams. *Earthquake Spectra*. 16:4, 775-798.

Hognestad, E., Hanson, N.W. and McHenry, D. (1955). "Concrete Stress Distribution in Ultimate Strength Design." *ACI Journal Proceedings*. 52:12, 455-479.

Liu, J., Sabelli, R., Brockenbrough, R.L. and Fraser, T.P. Expected Yield Stress and Tensile Strength Ratios for Determination of Expected Member Capacity in the 2005 AISC Seismic Provisions. *Engineering Journal*. First Quarter, 15-25.

Marcakis, K. and Mitchell, D. (1980). Precast Concrete Connections with Embedded Steel Members. *PCI Journal*. 25:4, 88-116.

Mattock, A.H. and Gaafar, G.H. (1982). Strength of Embedded Steel Sections as Brackets. *ACI Journal*. 79:9, 83-93.

Naish, D., Wallace, J.W., Fry, J.A. and Klemencic, R. (2009). Reinforced Concrete Link Beams: Alternative Details for Improved Construction. *UCLA – SGEL Report 2009/06*.

Shahrooz, B.M., Remetter, M.E. and Qin, F. (1993). Seismic Design and Performance of Composite Coupled Walls. *Journal of Structural Engineering*. 119:11, 3291-3309.

Wallace, J. W. (1992). BIAX: Revision 1-Computer program for the analysis of reinforced concrete and reinforced masonry sections. *Rep. No. CU/CEE-92/4, Structural Engineering, Mechanics, and Materials, Clarkson University, Potsdam, N.Y.*